Journal of Cluster Science
https://doi.org/10.1007/s10876-021-02099-0

ORIGINAL PAPER

Bioactive Molecules Coated Silver Oxide Nanoparticle Synthesis from *Curcuma zanthorrhiza* and HR-LCMS Monitored Validation of Its Photocatalytic Potency Towards Malachite Green Degradation

K. S. Aiswariya[1] · Vimala Jose[1]

Received: 6 February 2021 / Accepted: 20 May 2021

Abstract
The study focuses on a non-stringent, rapid and sustainable way for the synthesis of silver oxide nanoparticles (Ag_2ONPs) using aqueous rhizome extract of *Curcuma zanthorrhiza* Roxb. (Cz). High resolution liquid chromatography mass spectroscopy (HR-LCMS) was used for the simultaneous identification of bioactive molecules in the aqueous rhizome extract and its biosynthesized nanoparticles. The presence of eleven bioactive molecules in the rhizome extract acts as reducing and capping agents during the synthesis of Ag_2ONPs. The molecules coated to Ag_2ONPs were identified to be majorly sesquiterpenoids and lipid molecules. The analytical techniques used for the nanoparticle characterization included UV–Visible spectrum, which showed SPR band at 409 nm; FTIR spectrum depicted the bioactive molecules involved in capping and reduction of silver ions to silver oxide nanoparticles; XRD pattern attributed to fcc structure of $CzAg_2ONPs$ with an average size of 39.7 nm; HR-TEM and FESEM confirmed the size and morphology of $CzAg_2ONPs$. The chemical nature of the bioactive molecules bound to Ag_2ONPs revealed by HR-LCMS was in agreement with FTIR spectral data. The $CzAg_2ONPs$ exhibited efficient photocatalytic activity in the degradation of the toxic dye malachite green (MG) as revealed by the absorption spectra. The degraded product was subjected to HR-LCMS and found to be non-toxic. The results revealed the promising potential of bioactive molecules coated Ag_2ONPs for environmental cleanup.

Keywords Aqueous extract · Harminine · Coumarins · Photocatalyst · Benzophenone

Introduction

The tremendous increase in environmental pollution over the years can be attributed to the broad application of dyes in various industries and the imperfections in their removal. Currently, the commercial dyes have become an unavoidable substance in various industries and their management is of global concern. The highest discharge of dye effluents to the aqueous ecosystem, against the acceptable ecological norms are from the textile industry [1]. Residual dyes on reaching water bodies interfere with the sunlight penetration affecting photosynthesis, which eventually disturbs the ecosystem. Moreover, these effluents are potent toxins and carcinogens [2]. Due to the stability and persistence of the toxic pollutants in the environment, the development of appropriate treatments for the degradation of dye is necessary. The physicochemical techniques involved in the removal of dye from effluents are often very costly and the disposal of concentrated sludge creates a problem [3]. Time consumption and difficulty in degrading complicated dyes are the drawbacks of biological methods. Despite these challenges, the promising potential of nanotechnology enables the exploitation of nanoparticles and nanomaterials in environmental remediation.

Nanotechnology refers to the wide range of technologies and applications that involve the use of particles ranging from a few nanometers to hundreds of nanometers in diameter. Nanoparticles (NPs) have revolutionized the fields of environmental remediation, medicine, material science, chemistry and engineering. They have been exploited in catalysis, sensor technology, imaging, cancer

✉ Vimala Jose
vimalajoseparaemackel@gmail.com

[1] Centre for Bionanotechnology, Research and Post Graduate Department of Botany, St. Thomas' College, University of Calicut, Thrissur, Kerala 680001, India

Published online: 28 May 2021

treatments and site specific drug delivery because of their characteristic high surface to volume ratio compared to their bulk counterparts [4–8]. But the physicochemical processes involved in the synthesis of metallic nanoparticles involves the use of toxic solvents, posing a serious threat to the environment [9]. Therefore, in recent times, the use of natural materials such as microbes, parasites, yeast, seaweeds and plants as basic hotspot for the synthesis of metal nanoparticles has gained considerable interest among researchers[10, 11].

Plants are enriched with bioactive molecules which are unique in structure and function justifying their role in pharmaceutical, biomedical, nutraceutical, cosmeceutical, and chemical industries [12, 13]. Hence, the plants continue to be a critical source of present-day drugs [14–16]. The bioactive molecules have the potential to interact with various other compounds through a variety of chemical reactions. Apart from the pharmaceutical aspects, the tanning activity of plant polyphenols have been exploited in the leather industry [17]. In addition, the antibacterial and chelating capabilities of various plants and phytoplanktons have been used in the treatment of wastewater [18]. Despite the advantages of the biomolecules, the exploitation of the plant resources remains in a nascent stage. Consequently, during the recent years, synthesis of plant-based functional nanoparticles has evolved as a potential area of investigation among the scientific community [19]. Besides, the minimal efforts involved in synthesis, the plant material integrated nanoparticles do not have toxic materials on their surface and also show biocompatibility and biodegradability [20]. Moreover, the bioactive molecules act as reducing and stabilizing agents in the formation of metal nanoparticles [21, 22]. Therefore, the green synthesized nanoparticles have been explored in the field of nanoremediation. The green synthesized silver nanoparticles find its application in the degradation of pesticides, toxic dyes, as environmental sensors and mosquito control along with biological activities [23–31]. In this context, synthesis and application of silver and silver nanoparticle based materials has gained interest due to its morphology, biophysical properties and stability [32, 33].

However, the properties of the green synthesized nanoparticles not only depend on the phytoconstituents present in the plant but also the reaction conditions employed during the synthesis. Although synthesis of metallic nanoparticles utilizing plant's concentrates has been accounted for different plants, such as *Berberis vulgaris*, *Carica papaya*, *Ficus hispida*, *Ricinus communis var. carmencita*, *Combretum erythrophyllum*, *Morus indica*, *Mimusops coriacea*, *Zingiber officianale*, *Aspilia pluriseta*, *Caesalpinia pulcherrima*, *Sansevieria roxburghiana*, there is still a wide spectrum of plant metabolites yet to be investigated [34–43]. For instance, the rhizomes of *Curcuma zanthorrhiza* Roxb. (Cz) which are rich in curcuminoids, terpenoids, alkaloids, flavonoids, tannins, phenols and xanthorhizol, [44], have not yet been exploited in the synthesis of Ag_2ONPs. Moreover, the presence of these bioactive molecules accounts for its medicinal properties such as diuretic, anticancer, antioxidant, antibacterial, antifungal, anti-inflammatory and hepatoprotective effects [45–47].

Based on the above considerations, an attempt has been made to synthesize bioactive molecule coated silver oxide nanoparticles using the aqueous rhizome extract of *Curcuma zanthorrhiza* Roxb. The simultaneous identification of the plant derived biological molecules in the rhizome extract of Cz and the biosynthesized nanoparticles were examined using high resolution liquid chromatography mass spectroscopy (HR-LCMS). Different spectroscopic and electron microscopic techniques were used to characterize the physicochemical properties of the as-synthesized nanoparticles. Moreover, the photocatalytic efficiency of $CzAg_2$ONPs in the degradation of toxic dye malachite green (MG) was ascertained and the degradation products were subjected to HR-LCMS analysis.

Materials and Methods

Preparation of Plant Extract and Identification of Bioactive Molecules by HR-LCMS

Curcuma zanthorrhiza rhizomes (Fig. 1a) were multiplied from the original germplasm collection from the Regional station of National Bureau of Plant Genetic Resources (NBPGR), Thrissur, Kerala, India. It was cleaned, shade dried, powdered and stored. 10 g of this powder was boiled in 100 mL of deionised water for 30 min and filtered using Whatman No. 1 paper. The filtrate was further centrifuged at 5000 rpm and the supernatant was stored at 4 °C for future experiments.

The aqueous rhizome extract was subjected to bioactive molecule analysis by using high resolution liquid chromatograph mass spectrometer coupled to QTOF (HR-LCMS, Aligent Technologies, USA, 1290 Infinity UPHLC System, 6550 iFunnel QTOFs). The liquid chromatographic conditions employed in the bioactive molecule analysis are listed in Table 1. Mass spectra were generated in positive electrospray ionization mode (ESI).

Biosynthesis of Silver Oxide Nanoparticles ($CzAg_2$ONPs)

The aqueous rhizome extract was added to 1 mM silver nitrate solution, followed by irradiation of sunlight with continuous stirring for 30 min in Erlenmeyer flask. The

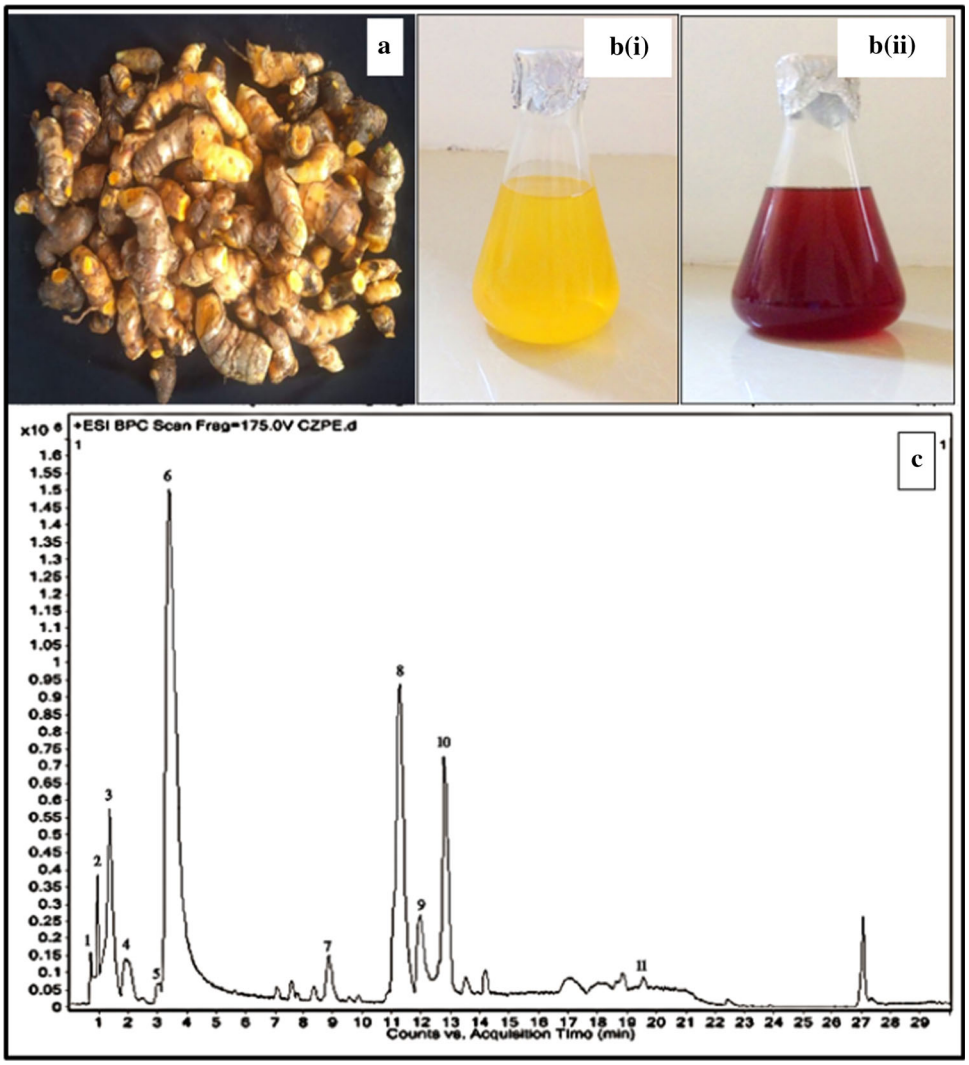

Fig. 1 **a** *Curcuma zanthorrhiza* rhizomes, **b** color change in reaction mixture from yellow to reddish brown indicated formation of Ag_2ONPs—(i) aqueous rhizome extract (yellow); (ii) biosynthesized $CzAg_2ONP$ suspension (reddish brown) and **c** HR-LCMS chromatogram of the aqueous rhizome extract of *C zanthorrhiza*. The peaks corresponds to bioactive molecules namely, norcotinine (peak 1, m/z = 185.0672), N-(1-deoxy-1-fructosyl) Valine (peak 2, m/z = 262.1308), ethyl 3-methyl-9H-carbazole-9-carboxylic acid (peak 3, m/z = 276.1463), feruperine (peak 4, m/z = 310.1306), gibberellic acid 19 (peak 5, m/z = 367.1526), harmanine (peak 6, m/z = 181.0779), gibberellic acid 3 (peak 7, m/z = 369.1358), obliquin (peak 8, m/z = 254.0829), pteryxin (peak 9, m/z = 369.1359), glechomafuran (peak 10, m/z = 231.14) and sinapoylspermine (peak 11, 391.2872) (Color figure online)

Table 1 Conditions employed during HR-LCMS measurement

Parameter	Condition
Column	Hypersil gold 3 micron, 100*2.1 mm (Aligent 1290 Infinity UHPLC)
Eluent types	90% Acetonitrile/10% water and 0.1% FA
Flow rate (mL min^{-1})	0.3
Injection volume (L)	3
Nebulizer pressure (psi)	35
Column temperature (°C)	25
Dry gas flow rate (L min^{-1})	13
Dry temperature (°C)	250
Vaporize temperature (°C)	300
Ion source	Positive ESI

ratio of rhizome extract to $AgNO_3$ was 1:10 by volume. The synthesized $CzAg_2ONPs$ were purified by repeated centrifugation at 12,000 rpm (Eppendorf 5430R) for 20 min followed by dispersion of pellet in deionized water to remove water-soluble biomolecules. The water suspended nanoparticles were oven dried and were used for all the further studies.

Characterization of Biosynthesized $CzAg_2ONPs$

The bioreduction of silver ions in the solution was monitored by measuring the UV–Visible spectra of the solution using UV–Visible spectrophotometer (Shimadzu UV probe 1800), at a resolution of 1 nm in the scanning range 600–300 nm using quartz cuvette of path length 1 cm. The X-ray diffraction (XRD) measurements were carried out on a PANalytical X-ray diffractometer at a scanning rate of 20 min^{-1} with an operating voltage of 40 kV and a current of 15 mA with Cu Kα radiation 1.5405 Å monochromatic filter in the angle range $2\theta = 10°–80°$. Ultra-thin film of $CzAg_2ONPs$ was prepared by dropping $CzAg_2ONP$ suspension on carbon coated copper grid. It was subsequently analyzed using high-resolution transmission electron microscope (HR-TEM, Tecnai G2, F30) operated at 300 kV was used to analyze the size and morphology of the nanoparticles. The topography of the nanoparticles as well as the elemental composition was studied by field emission scanning electron microscope-energy dispersive analysis of X rays (FESEM EDAX-Supra 55, Karl Zeiss) with an accelerating voltage of 20 kV. The bioactive molecules responsible for the reduction and stabilization of silver ions in the aqueous medium was investigated using FTIR Spectrophotometer (Thermo Nicolet, Avatar 370) with spectral range 4000–400 cm^{-1}, resolution 4 cm^{-1} and KBr pellets. Further, HR-LCMS spectra of the nanoparticle aqueous suspension was taken and compared against the HR-LCMS spectra of aqueous plant extract to ascertain the bound bioactive molecules in the synthesized nanoparticles.

Photocatalytic Degradation of Malachite Green (MG)

The photocatalytic activity of $CzAg_2ONPs$ in the degradation of MG in aqueous solution was evaluated as a model system for investigating nanoparticle efficiency in removing cationic dyes [1]. The aqueous solution of MG (10 mg L^{-1}) was treated with 100 µg L^{-1} of $CZAg_2ONPs$ and kept in dark for 30 min with continuous stirring prior to irradiation. The light source used for the irradiation was sunlight (600–800 µE m^{-2} s^{-1}) and UV lamp (30 W, 253 nm, Philips Holland) for duration of 4 h and 24 h, respectively in two sets of experimental conditions. At regular time intervals, 5 mL suspensions were taken from the two irradiation trials, centrifuged and the absorbance spectra were recorded using UV–Visible spectrophotometer [48]. The percentage of degradation was calculated using,

Percentage degradation = $(C_0 - C)/C_o \times 100$, C_0 is the concentration of dye prior to the reaction, C is the concentration of dye after the reaction.

MG solution (10 mg L^{-1}) was exposed to same physical conditions to serve as control in the experiment. The degraded products were further analyzed by HR-LCMS, with specified chromatographic conditions (Table 1).

Results and Discussions

Bioactive Molecules Analysis of Aqueous Rhizome Extract

The HR-LCMS analysis revealed the presence of eleven bioactive molecules in the aqueous rhizome extract of CZ (Fig. 1c). The bioactive molecules were identified based upon the spectral similarity with the MS library (NIST MS Search 2.0) and the Human Metabolome Database. The spectrometric data of the bioactive molecules including retention time, molecular mass, molecular formula, adduct ions formed in ion source and peak area percentage are listed in Table 2. The bioactive molecules identified by HR-LCMS analysis were norcotinine (peak 1, m/z = 185.0672), N-(1-deoxy-1-fructosyl) Valine (peak 2, m/z = 262.1308), ethyl 3-methyl-9H-carbazole-9-carboxylic acid (peak 3, m/z = 276.1463), feruperine (peak 4, m/z = 310.1306), gibberellic acid 19 (peak 5, m/z = 367.1526), harmanine (peak 6, m/z = 181.0779), gibberellic acid 3 (peak 7, m/z = 369.1358), obliquin (peak 8, m/z = 254.0829), pteryxin (peak 9, m/z = 369.1359), glechomafuran (peak 10, m/z = 231.14) and sinapoylspermine (peak 11, 391.2872) which belonged to the organic class of compounds namely, pyridine derivatives, fructose aminoacids, carbozoles, methoxy phenols, plant hormone, β carboline alkaloids, plant hormone, coumarins, germacrane furano sesquiterpenoids and hydroxycinnamic acid derivatives respectively. The germacrane type of sesquiterpenes are widely reported in the genus Curcuma [49]. The peak with m/z 231.14 corresponds to glechomafuran, a germacrane furano sesquiterpenoid, and this type of terpenoid has been reported in the rhizomes of *C. zedoaria* [50]. Hydroxycinnamic acid derivatives were also identified in the rhizomes of *C. domestica* [51]. However, the peak with m/z 391.287 was identified to be sinapoylspermine, a polyamine conjugated hydroxycinnamic acid [52].

The highest peak was identified to be of harminine, a β carboline alkaloid with a peak area of 35.33%, followed by obliquin, glechomafuran, ethyl 3-methyl-9H-carbazole-9-carboxylic acid, pteryxin, N-(1-deoxy-1-fructosyl) Valine, gibberellic acid 3, feruperine, sinapoylspermine, gibberellic acid 19 with peak area of 20%, 8.57%, 6.78%, 5.33%,

Table 2 Bioactive macromolecules in the aqueous rhizome extract of *Curcuma zanthorrhiza* identified from the HR-LCMS chromatogram presented in Fig. 1c

Peak No.	Retention time	Molecular mass (g/mol)	m/z	Formula	Adduct	Compound name	Peak area percentage (%)
1	0.762	162.0772	185.0672	$C_9H_{10}N_2O$	(M + Na)	Norcotinine (pyridine and derivatives)	0.37
2	1.147	279.134	262.1308	$C_{11}H_{21}NO_7$	(M + H-H_2O)	N-(1-deoxy-1-fructosyl)Valine (fructose aminoacid)	3.67
3	1.537	253.1571	276.1463	$C_{16}H_{15}NO_2$	(M + Na)	Ethyl 3-methyl-9H-carbazole-9-carboxylic acid (alkaloid)	6.78
4	1.896	287.1414	310.1306	$C_{17}H_{21}NO_3$	(M + Na)	Feruperine (methoxyphenols)	3.13
5	2.997	362.1739	367.1526	$C_{20}H_{26}O_6$	(M + Na-H_2O)	Gibberellic acid 19 (hormone)	0.77
6	3.227	198.0812	181.0779	$C_{12}H_{10}N_2O$	(M + H-H_2O)	Harmanine (alkaloid)	35.33
7	8.818	346.1472	369.1358	$C_{19}H_{22}O_6$	M + Na	Gibberellic acid 3 (hormone)	3.44
8	11.256	244.0757	245.0829	$C_{14}H_{12}O_4$	M + H	Obliquin (coumarins)	20.00
9	11.703	386.1393	369.1359	$C_{21}H_{22}O_7$	M + H-H_2O	Pteryxin (coumarins)	5.33
10	12.705	248.1433	231.14	$C_{12}H_{20}O_3$	M + H-H_2O	Glechomafuran (germacrane sesquiterpenoids)	8.57
11	19.626	408.2905	391.2872	$C_{21}H_{36}N_4O_2$	M + + H-H_2O	Sinapoylspermine (hydroxycinnamic acid derivatives)	1.10

3.67%, 3.44%, 3.13%, 1.1% and 0.77% respectively. Norcotinine, a pyrimidine derivative was quantified to be the least component present in the aqueous rhizome extract with an intensity of 0.37%. Moreover, harminine (m/z = 181.0779) was reported to be effective in the synthesis of silver nanoparticles and in pest management [53]. Major properties of bioactive compounds are given in Table 4. Furthermore, the coumarins, obliquin and pteryxin were identified for the first time in the aqueous rhizome extract of *C. zanthorrhiza*.

Biosynthesis of $CzAg_2ONPs$

Synthesis of $CzAg_2ONPs$ was observed by the addition of aqueous rhizome extract of *Curcuma zanthorrhiza* to 1 mM $AgNO_3$, kept under sunlight for 30 min. The color of the reaction mixture changed from pale yellow to reddish-brown color after 30 min irradiation, which indicated the formation of Ag_2ONPs at pH 5.65 (Fig. 1b). The excitation of surface vibration plasmon in the silver nanoparticles results in the change in color. A study by Hosseinpour et al., reported the requirement of 180 min for the formation of silver nanoparticles by thermal decomposition method [54]. However, in our study, the formation of Ag_2ONPs occurred more rapidly, where the whole reaction was completed within 30 min in an ambient condition.

Characterization of Biosynthesized $CZAg_2ONPs$

UV–Visible Spectroscopy

The formation of $CzAg_2ONPs$ was primarily characterized by UV–Visible Spectroscopy. In the UV spectrum, the broadening of peak indicated the particles are polydispersed in aqueous suspension [55]. According to Mie's theory, the absorption spectra of spherical nanoparticles show only a single Surface Plasmon Resonance (SPR) band. In the present study, the formed Ag_2ONPs was confirmed by UV–Visible spectrophotometer analysis. The UV–Visible spectra showed maximum absorption at 409 nm, with a single SPR band (Fig. 3a) revealing the spherical shape of Ag_2ONPs [56, 57]. The λ max of the aqueous rhizome extract was at 272.5 nm (Fig. 2).

X-ray Diffraction (XRD) Analysis

The XRD technique was used to determine and confirm the crystalline structure of Ag_2ONPs. Well defined characteristic diffraction peaks at 32.2, 38.1, 46.2, 54.63, 57.24, 64.98 and 76.54 corresponding to (111), (200), (211), (220), (221), (222) and (311) planes, respectively were identified, attributing to face-centred (fcc) crystal structure of metallic Ag_2ONPs (Fig. 3b). The XRD pattern of the biosynthesized $CzAg_2ONPs$ matched with the standard JCPDS file (No. 76-1393). Dhoondia and Chakraborty

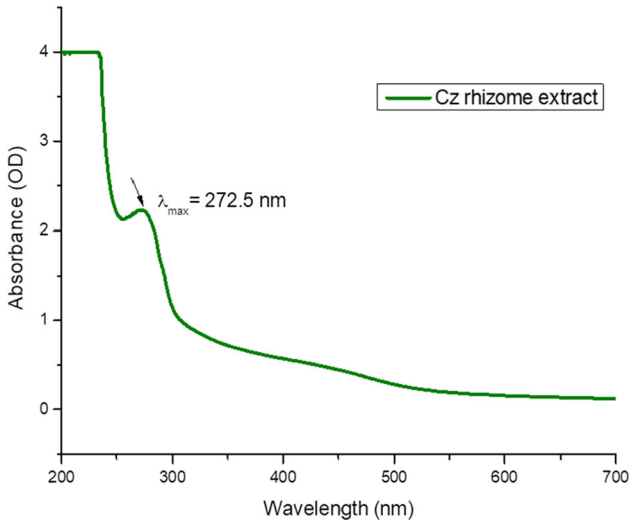

Fig. 2 The UV–Vis absorption spectrum of aqueous rhizome extract of *C. zanthorrhiza* (272.5 nm)

reported a similar finding on the formation of Ag_2ONPs using *Lactobacillus* [58]. In the present study, the average crystallite size calculated using the Scherrer equation for the biosynthesized $CzAg_2$ONPs were found to be 39.7 nm.

$$D = \frac{k\lambda}{\beta cos\theta}$$

where D is the average crystallite size, k = 0.94, λ is the X ray wavelength, β is the full width at half maxima (FWHM) and θ is the diffraction angle.

Electron Microscopy (HR-TEM and FESEM)

The HR-TEM micrographs revealed the spherical nature of the biosynthesized $CzAg_2$ONPs, which was in agreement with the UV data. The SAED pattern with bright circular spots indicated (111), (211), (220) and (311) planes and revealed the polycrystalline nature of nanoparticles, which was consistent with the XRD results obtained (Fig. 4b, c). The d spacing value of 0.276 nm observed is in agreement with the (111) lattice spacing of fcc silver (d_{111} = 0.2748) which further follows the standard JCPDS file (No. 76-1393). Further insight on the surface morphology of $CzAg_2$ONPs was obtained from FESEM micrographs. In agreement with the XRD results, the TEM and FESEM micrographs (Fig. 4a) also revealed the synthesized Ag_2-ONPs were spherical in shape with a diameter ranging from 17.98 to 46.73 nm.

Energy Dispersive Analysis of X-rays (EDAX)

The EDAX assists in finding out the elemental composition of the synthesized nanoparticles (Fig. 4d). The EDAX spectrum displayed the presence of elemental oxygen, silver with weight percentage 25.2%, 64.24%, respectively and the absence of elemental nitrogen confirming the reduction of silver nitrate to silver oxide nanoparticles. The presence of sharp and intense band peak at 3 keV is typical of the existence of metallic silver. Presence of signals for carbon in the spectrum is because of the biomolecules found in the rhizome extract that had been related with the synthesis of $CZAg_2$ONPs.

Fourier Transform Infrared (FTIR) Spectroscopy

The FTIR spectroscopic peaks showed the bioactive molecules in the aqueous rhizome extract responsible for the reduction of silver ions to metallic silver oxide nanoparticles, with prominent peaks at 3467.654, 2075.133, 1631.563, and 561.2115 cm^{-1} (Fig. 5). The spectrum showed the intense and broad absorption peak at 3467.654 denoting O–H stretching [29]. A strong and sharp

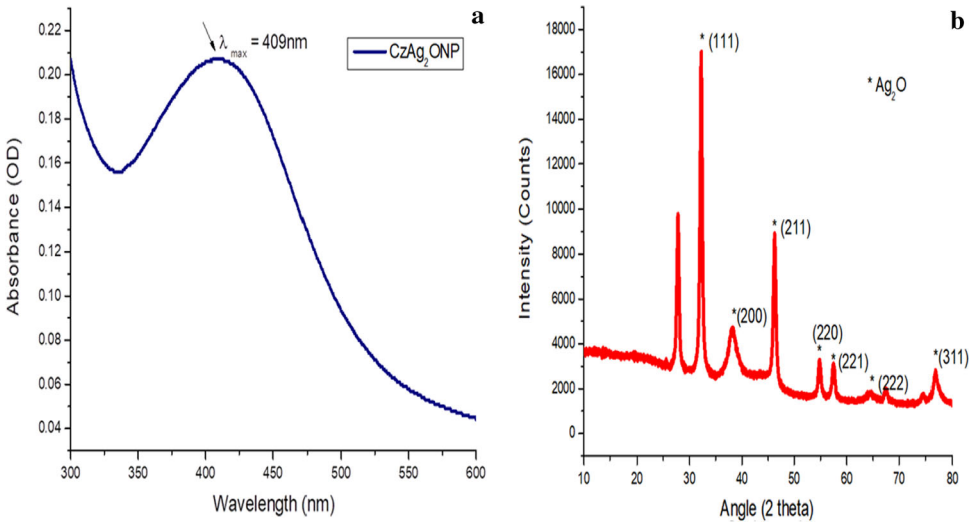

Fig. 3 **a** The UV–Vis absorption spectrum of $CzAg_2$ONPs (409 nm) synthesized with 0.1% (w/v) aqueous rhizome extract containing 1 mM $AgNO_3$ irradiated under sunlight for 30 min and **b** XRD pattern of $CzAg_2$ONPs synthesized from the aqueous rhizome extract attributed to fcc structure of metallic Ag_2ONPs with an average crystallite size 39.7 nm

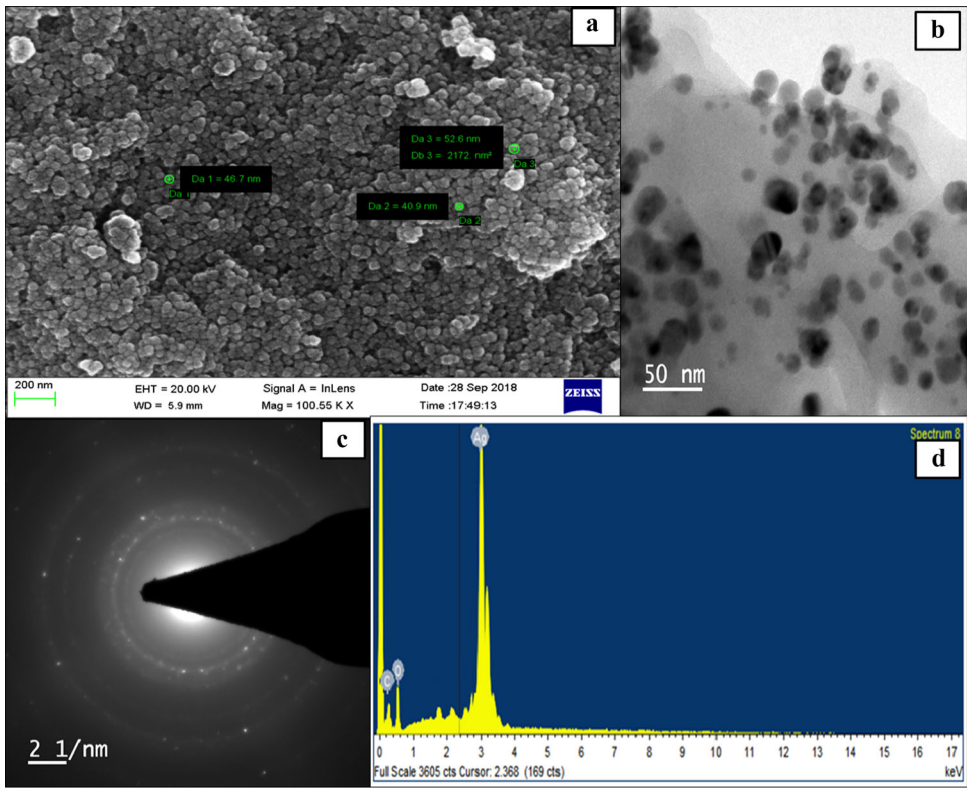

Fig. 4 **a** FESEM image of $CzAg_2ONPs$ biosynthesized from the aqueous rhizome extract denoting the spherical nature of the nanoparticles, **b** HR-TEM image of biosynthesized $CzAg_2ONPs$ revealed its spherical nature with size ranging from 17.98 to 46.73 nm, **c** SAED pattern attributing to the polycrystalline nature of $CzAg_2ONPs$ and **d** EDAX image of $CzAg_2ONPs$

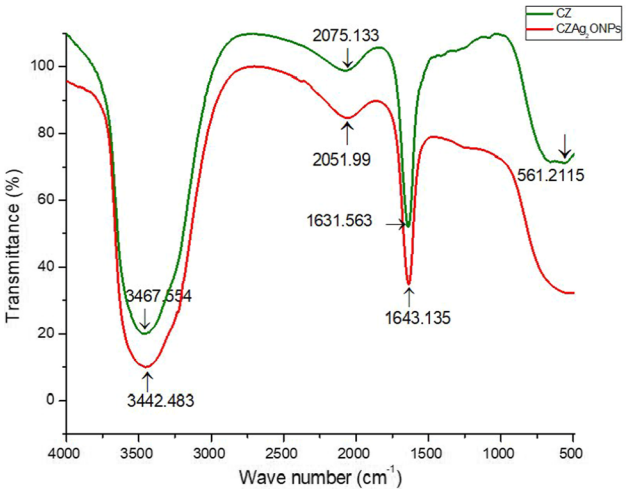

Fig. 5 FTIR spectra of the aqueous rhizome extract (CZ) and biosynthesized $CzAg_2ONPs$ with spectral range 4000–400 cm^{-1}

absorption band at 1631.563 cm^{-1} can be assigned to the stretching vibration of (NH) C = O group. Mariselvam et al. reported a similar finding which indicated the formation silver nanoparticles capped with biomoeties from the absorption band at 1638 cm^{-1} [59]. Furthermore, the peaks at 2075.133 and 561.2115 indicated the alkyne group in rhizome extract and C–Br stretching, respectively. For the biosynthesized $CzAg_2ONPs$, the characteristic bands were at 3442.483, 2051.99, 1643.135 $cm^{-1}$and absence of band around 500 cm^{-1}. There was a large shift in the peaks observed in $CzAg_2ONPs$, 3467.654 to 3442.483 cm^{-1}, 2075.133 to 2051.99 cm^{-1}, 1631.563 to 1643.135 cm^{-1} which indicated the involvement of hydroxyl groups, carboxyl amines, amino acid residues and alkyne derivatives which corresponds to carbohydrates, proteins and phenols, respectively. The bioactive molecules identified in the aqueous rhizome extract are listed in Table 2. However, from the IR spectrum results, it can be attributed that some of these bioactive molecules are involved in the reduction of silver nitrate to silver oxide nanoparticles [60, 61]. It is also reported that the biomolecules play a major role in reduction of gold chloride and capping with polymers improve their properties [62]. The amide linkage of proteins could be likely to form a coat over the $CzAg_2ONPs$, stabilizing them in the aqueous medium [63].

High Resolution Liquid Chromatography Mass spectroscopy (HR-LCMS)

The presence of six bioactive molecules were ascertained in the $CzAg_2ONP$ aqueous suspensions using the HR-LCMS analysis (Fig. 6) and these compounds were comparable with the HR-LCMS data of the aqueous rhizome extract (Fig. 1c). The bioactive molecules bound to Ag_2-ONPs were zedorone (peak 2, m/z = 229.1244), glechomafuran (peak 4, m/z = 231.1398) which belonged to

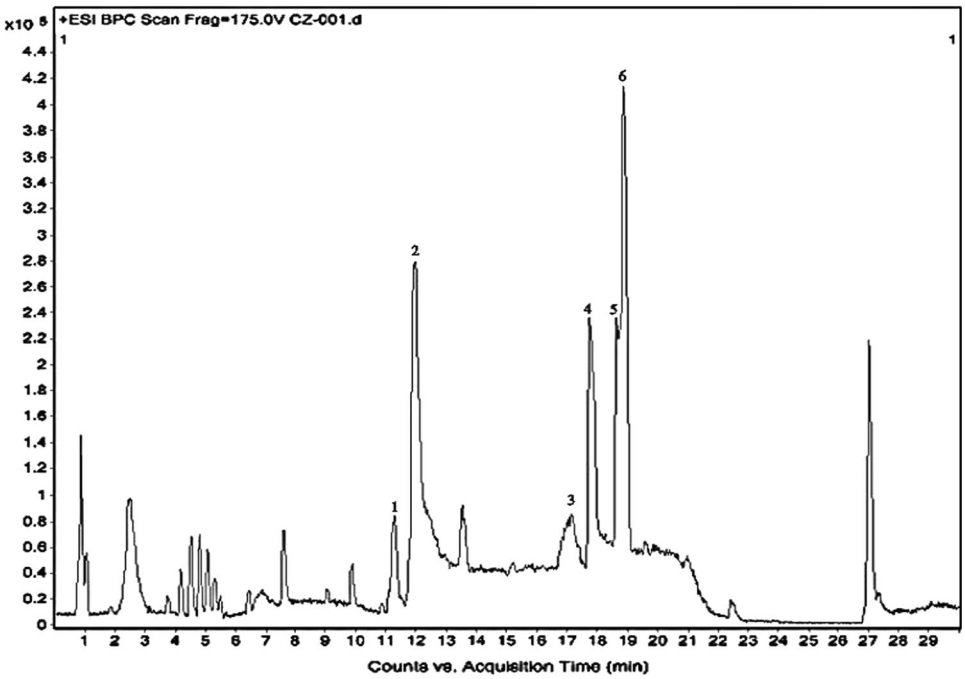

Fig. 6 HR-LCMS chromatogram of the biosynthesized silver oxide nanoparticle suspension. The bound bioactive molecules on $CzAg_2ONPs$ were tripeptide Val–His–Arg (peak 1, m/z = 415.217), zedorone (peak 2, m/z = 229.1244), 1-hexadecanoyl-sn-glycerol (peak 3, m/z = 313.2763), glechomafuran (peak 4, m/z = 231.1398), dihydrosphingosine (peak 5, m/z = 284.2973),and1-octadecanoyl-rac-glycerol (peak 6, m/z = 341.3073)

germacrene sesquiterpenoids, an aminoalcohol dihydrosphingosine (peak 5, m/z = 284.2973), two lipid molecules namely palmitoyl glycerol (1-hexadecanoyl-sn-glycerol) (peak 3, m/z = 313.2763), stearoyl glycerol (1-octadecanoyl-rac-glycerol) (peak 6, m/z = 341.3073) and tripeptide Val–His–Arg (peak 1, m/z = 415.217) and were quantified to 15.04%, 8.79%, 8.17%, 10.55%, 14.28% and 3.51%, respectively. The retention time, adduct ions formed in ion source, molecular mass, molecular formula and peak area percentage of the bioactive molecules are listed in Table 3. This result ascertains the presence of bound bioactive molecules in the biosynthesized $CzAg_2ONPs$ which corroborates with the FTIR results.

Photocatalytic Degradation of MG

The drop in the characteristic absorption peak of MG at 615 nm was used as an indicator for examining the degradation of the dye catalyzed by $CzAg_2ONPs$. There was a gradual decrease in the main absorption peak of MG with the increase in exposure time to sunlight and UV light (Fig. 7a, b). The sunlight exposed dye-nanoparticle

Table 3 Bioactive macromolecules coated on $CzAg_2ONPs$ identified from the HR-LCMS Chromatogram presented in Fig. 6

Peak No	Retention time	Molecular mass (g/mol)	m/z	Formula	Adduct	Compound name	Peak area percentage (%)
1	11.8	410.236	415.217	$C_{17}H_{30}N_8O_4$	(M + Na-H_2O)	Val–His–Arg (tripeptide)	3.51
2	12.245	246.129	229.124	$C_{15}H_{18}O_3$	(M + H-H_2O)	Zedorone (Germacrane sesquiterpenoids)	15.04
3	17.332	330.279	313.276	$C_{19}H_{38}O_4$	(M + H-H_2O)	1-hexadecanoyl-sn-glycerol	10.55
4	17.734	248.143	248.297	$C_{15}H_{20}O_3$	(M + H-H_2O)	Glechomafuran (Germacrane sesquiterpenoids)	8.79
5	18.641	301.300	284.297	$C_{18}H_{39}NO_2$	(M + H-H_2O)	Dihydrosphingosine (aminoalcohol)	8.17
6	18.82	358.310	341.307	$C_{21}H_{42}O_4$	(M + H-H_2O)	1-octadecanoyl-rac-glycerol	14.28

The phytoconstituents were identified based upon spectral similarity with the MS library (NIST MS Search 2.0) and the Human Metabolome Database

suspension had quick de-colorization (4 h) compared to UV light (24 h) exposed suspension. The percentage of degradation of MG was 94.7% under sunlight and 22.83% upon UV irradiation.

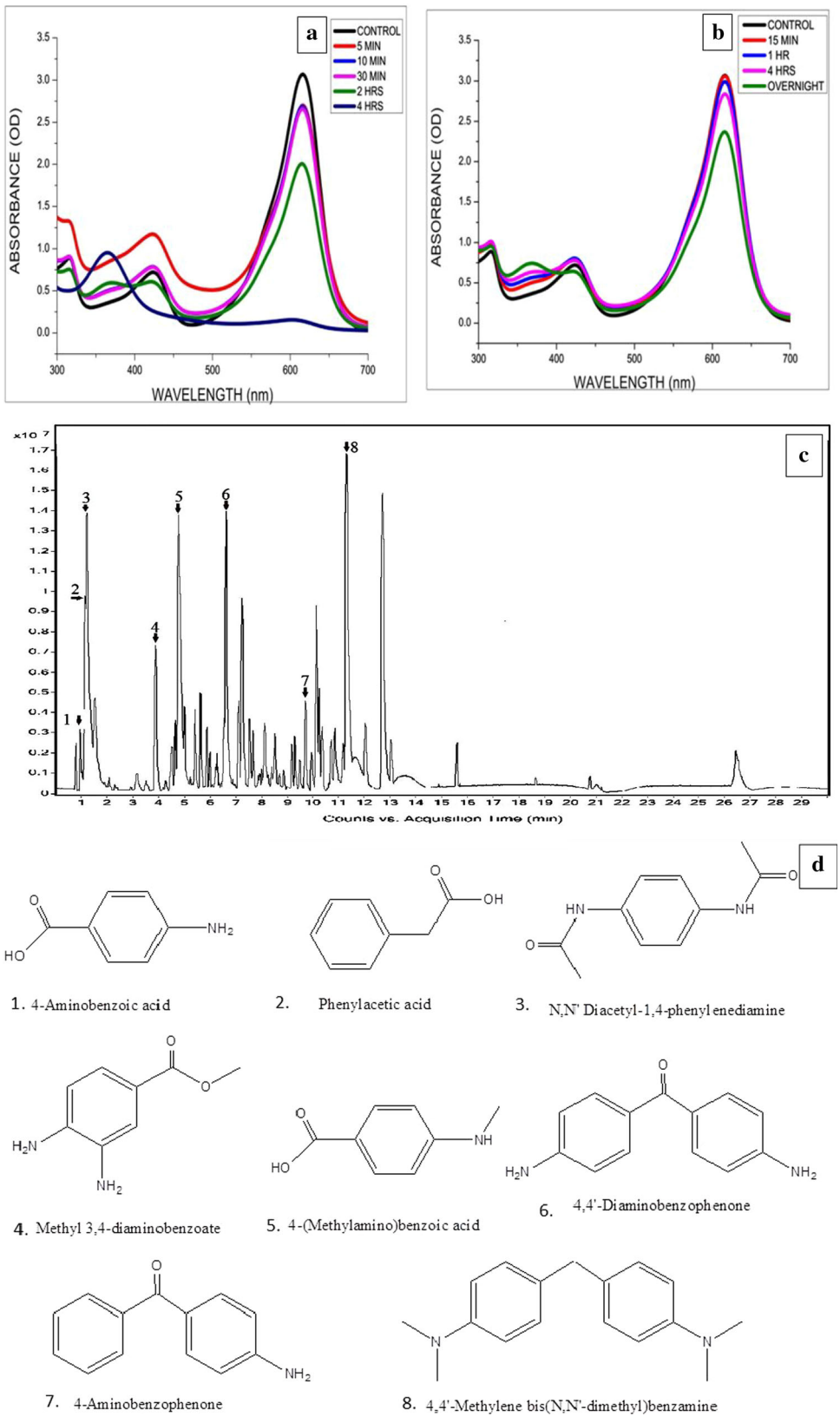

Fig. 7 UV–Visible spectra of decomposition of MG dye using $CzAg_2ONPs$ as photocatalysts: **a** under sunlight (94.7% degradation) **b** under UV light (22.83% degradation), **c** HR-LCMS chromatogram of MG treated with $CzAg_2ONPs$ after irradiation with sunlight and **d** its degradation products—(1) 4-amino benzoic acid (m/z 137.04, 1.08%), (2) phenylacetic acid (m/z 192.09, 7.99%), (3) N,N′ diacetyl 1,4 phenylene diamine (m/z 192.09, 11.46%), (4) methyl 3,4 di amino benzoate (m/z 166.07, 4.85%), (5) 4-methyl amino benzoic acid (m/z 151.06, 11.43%), (6) 4,4′ diamino benzophenone (m/z 212.09, 6.89%), (7) 4-amino benzophenone (m/z 197.08, 0.75%) and (8) 4,4′ methylene bis (N,N′dimethyl) benzamine (m/z 254.18, 11.09%)

Table 4 Bioactive compounds and their properties

Bioactive Compounds	Properties	References
Norcotinine	Neuropharmalogical property	[68]
Feruperine	Antioxidant activity	[69]
Harmanine	Insecticidal property	[53]
Obliquin	Anti-depressive activity	[70]
Pteryxin	Vasorelaxant, hepatoprotective, treatment of Alzheimer's disease	[71]
Glechomafuran	Antioxidant, anticancer activity	[72]
Sinapoylspermine	Anti-inflammatory, neuroprotective, antioxidant, anticancer, antimicrobial, cosmetic	[73]
Zedorone	Antioxidant, anticancer, antimicrobial, carminative, analgesic, insecticide	[74]

The degradation product when subjected to HR-LCMS analysis displayed the possible intermediates formed during the breakdown of MG. The retention time of the control dye MG is at 11.585, which was different from the retention time of all the degraded products in the range of 1.02–11.447 (Fig. 7c). The HR-LCMS analysis of MG and degradation products confirmed the efficacy of bioactive molecule coated $CzAg_2ONPs$ as good photocatalysts in the effective removal of the model dye. The reaction showed no progress in the absence of nanocatalysts (control). The HR-LCMS analysis of reaction product of MG-nanoparticle suspension showed the presence of compounds with molecular weights 137.04, 136.03, 192.09, 166.07, 151.06, 212.09, 197.08 and 254.18 m/z which could be interpreted as structures of 4-aminobenzoic acid, phenylacetic acid, N, N′ diacetyl 1,4 phenylene diamine, methyl 3,4 di aminobenzoate, 4-methyl aminobenzoic acid, 4,4′ diamino benzophenone, 4-amino benzophenone and 4,4′ methylene bis (N,N'dimethyl) benzamine, respectively (Fig. 7d), whereas the molecular weight of MG dye is 330.20 m/z. Out of the eight intermediates formed during the breakdown of MG, N,N′ diacetyl 1,4 phenylene diamine was quantified to be the most abundant degradation product (11.46%), followed by 4-methyl aminobenzoic acid (11.43%), 4,4′ methylene bis (N,N′ dimethyl) benzamine (11.09%), phenylacetic acid (7.99%), 4,4′ diamino benzophenone (4.85%), 4-aminobenzoic acid (1.08%) and 4-amino benzophenone (0.75%).

The formation of benzophenone derivatives by N-demethylation of MG have been reported as one of the major reaction involved in photo-oxidative process [64]. This is in agreement with our obtained results, since most of the products identified after degradation was derivatives of benzophenone. The possible mechanism of degradation may be due to the generation of hydroxyl radicals by the highly energetic electrons released when the photons struck the valence electrons of the molecule capped $CzAg_2ONPs$ [65]. These low molecular weight structures being mostly benzene derivatives may further be decomposed to form small organic molecules which eventually breaks down into CO_2 and H_2O [66]. Moreover, the formation of highly toxic leucomalachite green, a reduced form of MG was not detected in our study ascertaining the non-toxic dye removal process by bioactive molecule coated $CzAg_2$-ONPs, rendering unhazardous products to the environment [67] (Table 4).

Conclusion

The promising potential of the aqueous rhizome extract of *Curcuma zanthorrhiza* was for the first time exploited in a non-stringent and sustainable way for the synthesis of bioactive molecule coated silver oxide nanoparticles. The bioactive molecules present in the aqueous rhizome extract were identified by HR-LCMS analysis. The analytical capabilities of different spectroscopic techniques like UV–Visible Spectroscopy, FTIR, XRD and HR-LCMS were used to detect, identify, quantify and characterize the nanoparticles. The size and morphology of the nanoparticles were ascertained by HR-TEM and FESEM-EDAX. Among the different available analytical tools used for the characterization of biosynthesized nanoparticles, HR-LCMS offers remarkable capacities for the identification and quantification of associated molecules in the nanoparticles. The $CzAg_2ONPs$ proved outstanding photocatalytic efficacy in the debasement of toxic dye, MG. HR-LCMS analysis indicated degradation of MG after the $CzAg_2ONP$ treatment, whereas no change of MG was found in the control. By integrating HR-LCMS with the UV–Visible Spectroscopy, conclusive evidences were achieved for the photocatalytic degradation of MG, ultimately formulating a bioremediation protocol. Therefore, the results proved promising potential of *Curcuma zanthorrhiza* derived bioactive molecule coated Ag_2ONPs in the degradation of MG. Further, we could also develop a

simple and sensitive HR-LCMS mediated protocol for the detection and quantification of molecules in the nanoparticles and its degradation products.

Acknowledgements We gratefully acknowledge Council of Science and Industrial Research (CSIR) [File No. 08/633(0005)/2017-EMR-1], Government of India for the fellowship; DST-FIST for the facilities at St. Thomas' College (Autonomous), Thrissur, Kerala, India; SAIF at IIT Bombay, India for HR-TEM and LCMS measurements; Centre for Nanoscience and Nanotechnology, Sathyabama University, Chennai, Tamil Nadu, India for FESEM measurements; STIC Cochin University, Kerala, India for FTIR analysis and Kerala Veterinary and Animal Science University, Thrissur, Kerala, India for Lyophilisation technique.

Author Contributions AKS: Methodology, formal analysis, investigation, data curation, validation, software, writing—original draft. VJ: Conceptualisation, supervision, visualisation, writing—review and editing.

Funding No funds, grants or other support was received.

Declaration

Conflict of interest The authors have no conflict of interest to declare that are relevant to the content of this article.

References

1. X. Wang, Y. F. Zheng, H. Y. Yin, and X. C. Song (2011). *J. Nanosci. Nanotechnol.* **11**, 2501.
2. F. Deniz and R. Kepekci (2017). *Microchem. J.* **132**, 172.
3. T. Robinson, G. McMullan, R. Marchant, and P. Nigam (2001). *Bioresour. Technol.* **77**, 247.
4. N. Norouzi, M. K. Das, A. J. Richard, A. A. Ibrahim, H. M. El-Kaderi, and S. El-Shall (2020). *Nanoscale* **12**, 19191.
5. P. Prosposito, L. Burratti, and I. Venditti (2020). *Chemosensors* **8**, 1.
6. L. L. Israel, A. Galstyan, E. Holler, and J. Y. Ljubimova (2020). *J. Control. Release* **320**, 45.
7. F. Ren, H. Liu, H. Zhang, Z. Jiang, B. Xia, C. Genevois, T. He, M. Allix, Q. Sun, Z. Li, and M. Gao (2020). *Nano Today* **34**, 100905.
8. M. Gisbert-Garzarán, J. C. Berkmann, D. Giasafaki, D. Lozano, K. Spyrou, M. Manzano, T. Steriotis, G. N. Duda, K. Schmidt-Bleek, G. Charalambopoulou, and M. Vallet-Regí (2020). *ACS Appl. Mater. Interfaces* **12**, 14946.
9. K. D. Lee and P. C. Nagajyothi (2011). *J. Nanomater.* **2011**, 557.
10. P. B. Dayma, A. V. Mangrola, S. P. Suriyaraj, P. Dudhagara, and K. Rajesh (2019). *J. Pharm. Chem. Biol. Sci.* **7**, 94.
11. S. Mohan, O. S. Oluwafemi, S. P. Songca, V. P. Jayachandran, D. Rouxel, O. Joubert, N. Kalarikkal, and S. Thomas (2016). *J. Mol. Liq.* **213**, 75.
12. M. Bilal and H. M. N. Iqbal (2020). *Int. J. Biol. Macromol.* **151**, 1.
13. S. M. Amini (2019). *Mater. Sci. Eng. C* **103**, 109809.
14. P. J. Delaquis, K. Stanich, B. Girard, and G. Mazza (2002). *Int. J. Food Microbiol.* **74**, 101.
15. R. H. Liu (2003). *Am. J. Clin. Nutr.* **78**, 3.
16. S. E. Cross, Y. S. Jin, Q. Y. Lu, J. Rao, and J. K. Gimzewski, Nanotechnology 22, (2011).
17. S. Quideau, D. Deffieux, C. Douat-Casassus, and L. Pouységu (2011). *Angew. Chem. Int. Ed.* **50**, 586.
18. O. OoKolawole, S. Oguntoye, O. Agbede, and A. Olayemi (2006). *Ethnobot. Leafl.* **10**, 228.
19. C. L. Criado (2015). *J. Nanomed. Res.* **2**, 2.
20. M. Ovais, A. T. Khalil, A. Raza, M. A. Khan, I. Ahmad, N. U. Islam, M. Saravanan, M. F. Ubaid, M. Ali, and Z. K. Shinwari (2016). *Nanomedicine* **12**, 3157.
21. R. M. H. Shoker (2020). *Int. J. Res. Appl. Sci. Biotechnol.* **7**, 354.
22. N. Anwar, A. Khan, M. Shah, A. Azam, K. Zaman, and Z. Parven (2016). *Russ. J. Phys. Chem. A* **90**, 2625.
23. N. A. Ramos-Delgado, L. Hinojosa-Reyes, I. L. Guzman-Mar, M. A. Gracia-Pinilla, and A. Hernández-Ramírez (2013). *Catal. Today* **209**, 35.
24. U. Kamran, H. N. Bhatti, M. Iqbal, S. Jamil, and M. Zahid (2019). *J. Mol. Struct.* **1179**, 532.
25. T. Rasheed, F. Nabeel, M. Bilal, and H. M. N. Iqbal (2019). *Biocatal. Agric. Biotechnol.* **19**, 101154.
26. K. Farhadi, M. Forough, R. Molaei, S. Hajizadeh, and A. Rafipour (2012). *Sens. Actuators B Chem.* **161**, 880.
27. K. B. A. Ahmed, R. Senthilnathan, S. Megarajan, and V. Anbazhagan (2015). *J. Photochem. Photobiol. B Biol.* **151**, 39.
28. K. Velayutham, R. Ramanibai, and M. Umadevi (2016). *J. Basic Appl. Zool.* **74**, 37.
29. D. A. Aina, O. Owolo, A. Lateef, F. O. Aina, and A. S. Hakeem (2019). *Karbala Int. J. Mod. Sci.* **5**, 2.
30. M. Arshad, A. Khan, Z. H. Farooqi, M. Usman, M. Abdul Waseem, S. A. Shah, and M. Khan (2018). *Mater. Sci. Pol.* **36**, 21.
31. K. S. Aiswariya and V. Jose (2021). *J. Inorg. Organomet. Polym. Mater.* https://doi.org/10.1007/s10904-021-01951-0.
32. A. Syafiuddin, Salmiati, M. R. Salim, A. Beng Hong Kueh, T. Hadibarata, and H. Nur (2017). *J. Chin. Chem. Soc.* **64**, 732.
33. L. P. Silva, T. M. Pereira, and C. C. Bonatto, *Frontiers and Perspectives in the Green Synthesis of Silver Nanoparticles* (Elsevier Inc., Amsterdam, 2019).
34. M. Behravan, A. Hossein Panahi, A. Naghizadeh, M. Ziaee, R. Mahdavi, and A. Mirzapour (2019). *Int. J. Biol. Macromol.* **124**, 148.
35. A. V. Ramesh, D. R. Devi, G. R. Battu, and K. Basavaiah (2018). *S. Afr. J Chem. Eng.* **26**, 25.
36. S. Ojha, A. Sett, and U. Bora (2017). *Adv. Nat. Sci. Nanosci. Nanotechnol.* **8**, 035009.
37. O. T. Jemilugba, E. H. M. Sakho, S. Parani, V. Mavumengwana, and O. S. Oluwafemi (2019). *Colloids Interface Sci. Commun.* **31**, 100191.
38. S. Some, O. Bulut, K. Biswas, A. Kumar, A. Roy, I. K. Sen, A. Mandal, O. L. Franco, İA. İnce, K. Neog, S. Das, S. Pradhan, S. Dutta, D. Bhattacharjya, S. Saha, P. K. Das Mohapatra, A. Bhuimali, B. G. Unni, A. Kati, A. K. Mandal, M. D. Yilmaz, and I. Ocsoy (2019). *Sci. Rep.* **9**, 1.
39. C. R. B. Lopes and L. C. Courrol (2018). *J. Lumin.* **199**, 183.
40. A. R. M. Abd El-Aziz and M. R. Al-Othman (2019). *Pakistan J. Bot.* **51**, 443.
41. A. O. Nyabola, P. G. Kareru, E. S. Madivoli, S. I. Wanakai, and E. G. Maina (2020). *J. Inorg. Organomet. Polym. Mater.* **30**, 3493.
42. P. Moteriya and S. Chanda (2020). *J. Inorg. Organomet. Polym. Mater.* **30**, 3920.
43. A. G. Rama Krishna, C. S. Espenti, Y. V. Rami Reddy, A. Obbu, and M. V. Satyanarayana (2020). *J. Inorg. Organomet. Polym. Mater.* **30**, 4155.
44. H. P. A. Mary, G. K. Susheela, S. Jayasree, A. M. Nizzy, B. Rajagopal, and S. Jeeva (2012). *Asian Pac. J. Trop. Biomed.* **2**, S637.
45. C. Singgih Wahono, C. Diah Setyorini, H. Kalim, N. Nurdiana, and K. Handono (2017). *Int. J. Rheumatol.* **2017**, 1.

46. Y. H. Cheah, F. J. Nordin, R. Sarip, T. T. Tee, H. L. P. Azimahtol, H. M. Sirat, B. A. A. Rashid, N. R. Abdullah, and Z. Ismail (2009). *Cancer Cell Int.* **9**, 1.
47. S. Anjusha and A. Gangaprasad (2014). *J. Pharmacogn. Phytochem.* **3**, 50.
48. T. J. I. Edison and M. G. Sethuraman (2012). *Process Biochem.* **47**, 1351.
49. W. Sun, S. Wang, W. Zhao, C. Wu, S. Guo, H. Gao, H. Tao, J. Lu, Y. Wang, and X. Chen (2017). *Crit. Rev. Food Sci. Nutr.* **57**, 1451.
50. H. Shibuya, Y. Cai, I. Kitagawa, and Y. Hamamoto (1987). *Chem. Pharm. Bull.* **35**, 924.
51. D. Herebian, J. H. Choi, A. M. Abd El-Aty, J. H. Shim, and M. Spiteller (2009). *Biomed. Chromatogr.* **23**, 951.
52. J. Luo, C. Fuell, A. Parr, L. Hill, P. Bailey, K. Elliott, S. A. Fairhurst, C. Martin, and A. J. Michael (2009). *Plant Cell* **21**, 318.
53. A. A. Almadiy, G. E. Nenaah, and D. M. Shawer (2018). *J. Pest Sci. (2004)* **91**, 727.
54. S. M. Hosseinpour-mashkani and M. Ramezani (2014). *Mater. Lett.* **130**, 259.
55. S. Bhowmik, B. K. Datta, A. K. Saha, P. Chakma, and N. C. Mandal (2016). *Not. Sci. Biol.* **8**, 106.
56. W. Chengzheng, W. Jiazhi, C. Shuangjiang, M. K. Swamy, U. R. Sinniah, M. S. Akhtar, and A. Umar (2018). *J. Nanosci. Nanotechnol.* **18**, 3673.
57. W. R. Rolim, M. T. Pelegrino, B. de Araújo Lima, L. S. Ferraz, F. N. Costa, J. S. Bernardes, T. Rodigues, M. Brocchi, and A. B. Seabra (2019). *Appl. Surf. Sci.* **463**, 66.
58. Z. H. Dhoondia and H. Chakraborty (2012). *Nanomater. Nanotechnol.* **2**, 15.
59. R. Mariselvam, A. J. A. Ranjitsingh, C. Thamaraiselvi, and S. Ignacimuthu (2019). *J. King Saud Univ. Sci.* **31**, 1363.
60. S. P. Dubey, M. Lahtinen, and M. Sillanpää (2010). *Process Biochem.* **45**, 1065.
61. R. Mata, J. Reddy Nakkala, and S. Rani Sadras (2015). *Mater. Sci. Eng. C* **51**, 216.
62. N. Anwar, J. Wahid, J. Uddin, A. Khan, M. Shah, S. A. Shah, F. Subhan, M. A. Khan, K. Ali, M. Rauf, and M. Arif (2021). *Vitr. Cell. Dev. Biol. Plant* **57**, 248.
63. S. Priyadarshini, V. Gopinath, N. Meera Priyadharsshini, D. Mubarak Ali, and P. Velusamy (2013). *Colloid Surf. B* **102**, 232.
64. L. A. Pérez-Estrada, A. Agüera, M. D. Hernando, S. Malato, and A. R. Fernández-Alba (2008). *Chemosphere* **70**, 2068.
65. L. Wang, F. Lu, Y. Liu, Y. Wu, and Z. Wu (2018). *J. Mol. Liq.* **263**, 187.
66. Y. M. Ju, S. G. Yang, Y. C. Ding, C. Sun, C. G. Gu, Z. He, C. Qin, H. He, and B. Xu (2009). *J. Hazard. Mater.* **171**, 123.
67. S. S. Sutar, P. J. Patil, A. S. Tamboli, D. N. Patil, O. A. Apine, and J. P. Jadhav (2019). *Biocatal. Agric. Biotechnol.* **20**, 101183.
68. P. A. Crooks, M. Li, and L. P. Dwoskin (1997). *Drug Metab. Dispos.* **25**, 47.
69. N. Nakatani, R. Inatani, H. Ohta, and A. Nishioka (1986). *Environ. Health Perspect.* **67**, 135.
70. H. M. P. Poumale, R. Hamm, Y. Zang, Y. Shiono, and V. Kuete, *Coumarins and Related Compounds from the Medicinal Plants of Africa* (Elsevier, Amsterdam, 2013).
71. I. E. Orhan, F. S. Senol, S. Shekfeh, K. Skalicka-Wozniak, and E. Banoglu (2017). *Food Chem. Toxicol.* **109**, 970.
72. L. Quassinti, M. Bramucci, G. Lupidi, L. Barboni, M. Ricciutelli, G. Sagratini, F. Papa, G. Caprioli, D. Petrelli, L. A. Vitali, S. Vittori, and F. Maggi (2013). *Food Chem.* **138**, 808.
73. M. Roumani, R. E. Duval, A. Ropars, A. Risler, C. Robin, and R. Larbat (2020). *Biomed. Pharmacother.* **131**, 110762.
74. M. Soonwera, O. Wongnet, and S. Sittichok (2018). *Phytomedicine* **47**, 93.